Prior information in fluorescence molecular tomography based on multispectral fluorescence emission

Axelsson, Johan; Svensson, Jenny; Andersson-Engels, Stefan

Published in:
Progress in Biomedical Optics and Imaging - Proceedings of SPIE

DOI:
10.1117/12.699464

2007

Prior information in fluorescence molecular tomography based on multispectral fluorescence emission

J. Axelsson*, J. Svensson, S. Andersson-Engels
Department of Physics, Lund University, P.O. Box 118, SE-221 00 Lund, Sweden.

ABSTRACT

Fluorescence molecular tomography (FMT) suffers from inherent ill-posedness due to the vast number of possible solutions to the reconstruction problem. To increase the robustness of such a problem one need prior information. We present here a method for rendering *a priori* information of the position of a fluorescent inclusion inside turbid media. The method utilizes solely two spectral bands within the fluorescence spectrum emitted from the fluorophore. The method is presented and verified using experimental data from a tissue phantom. The confinement is also used to impose weights onto the voxels before the inversion of the linear set of equations describing the FMT problem.

Keywords: Fluorescence molecular tomography, fluorescence spectroscopy, a priori information, reconstruction schemes

1. INTRODUCTION

Fluorescence molecular tomography (FMT) has evolved during the last years to become an important method to image fluorescent markers deep inside biological media. The fluorescent markers attached to specific biological molecules provide means to monitor disease and treatment progression *in vivo* in small animals[1]. In an FMT setup laser light is delivered onto several positions on the surface of the imaged volume. The excitation light is diffusely propagating into the medium and will induce fluorescence wherever a fluorescent marker is positioned. Following the excitation the fluorophore will almost instantaneously emit fluorescent light, within the characteristic fluorescence spectrum of the fluorophore. The emission propagates through the medium and is collected by a detector placed at the boundary. Application of multiple detectors placed at different locations on the boundary will yield information about the intensity distribution of the light escaping from the tissue surface.

Recent advances within the development of FMT systems have rendered the use of non-contact detection schemes[2] providing the possibility for high resolution fluorophore reconstruction[3]. Using non-contact detection schemes drastically increases the size of the data set used for reconstruction, thus the reconstruction geometry should be optimally defined based on the balance between computational cost and resolution[4]. In addition the tomographic reconstruction is mathematically ill-conditioned yielding multiple non-unique solutions satisfying the recorded signals. Hence there is a need for prior information that demarcates the most probable fluorophore position in order to increase the robustness. To select a feasible reconstruction region *a priori* information based on MR images in combination with diffuse optical tomography has been reported[5].

In this proceeding we present a simple method based on solely the fluorescent emission, from a fluorophore, to render prior information about the inclusion position. The method is verified using experimental data retrieved from an optical phantom and a simple FMT system.

2. MATERIAL AND METHODS

2.1 Experimental setup

The experimental setup is schematically depicted in Fig. 1. The imaged geometry was a slab-shaped glass cuvette filled with a tissue phantom solution consisting of 1.1% Intralipid and water. As absorber 0.4%

Optical Tomography and Spectroscopy of Tissue VII
edited by Britton Chance, Robert R. Alfano, Bruce Jason Tromberg, Mamoru Tamura, Eva Marie Sevick-Muraca
Proc. of SPIE Vol. 6434, 64340D, (2007) · 1605-7422/07/$18 · doi: 10.1117/12.699464

bovine blood was added to the solution. The optical properties, shown in Table 1, of the bulk tissue phantom were assessed using an integrating sphere setup[6].

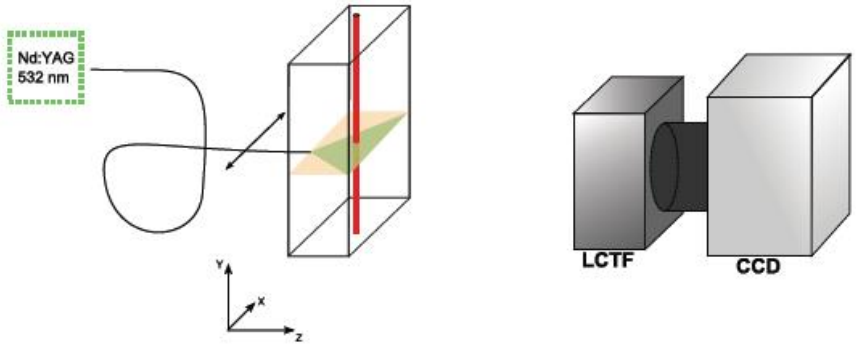

Figure 1. Schematic illustration of the experimental setup

The fluorescent inclusion was a cylinder with the inner diameter 5.6 mm filled with 0.5 μM or 1 μM Rhodamine 6G mixed with the phantom solution.

The excitation light source was a Nd:YAG laser (Millenia Vs, Spectra Physics Laser) emitting at 532 nm. The laser light was coupled into an optical fiber with the fiber tip placed in close contact with the glass surface of the slab. The excitation light power was 80 mW. The induced fluorescence was collected at the opposite boundary by a CCD (Hamamatsu, C4742-80-12 AG) equipped with an objective lens (Nikon, f/1.8, focal length 50 mm). A liquid crystal tunable filter (LCTF, Varispec LCTF VIS 20-35) was placed in front of the camera objective in order to filter the incident light into different spectral bands. The filter FWHM was 20 nm. Two spectral bands within the fluorescent emission profile, centered at λ_{m1}=560 nm and λ_{m1}=600 nm, were imaged.

Table 1. Optical properties of the bulk phantom

	μ_a (1/cm)	μ_s' (1/cm)
(λ_x) 532 nm	0.78	14
(λ_{m1}) 560 nm	0.59	13
(λ_{m2}) 600 nm	0.29	12

The excitation light source was delivered onto the phantom boundary at 10 different source positions and the detected light was extracted from the images acquired by the CCD-camera. A total of 31 simulated detectors were extracted from the image equally spaced along the x-axis.

The relative intrinsic emission spectrum of the fluorophore was measured with a spectrometer (OceanOptics, USB4000) for a solution of Rhodamine 6G of low concentration. The emission spectrum was normalized with the maximum intensity and the relative quantum yield for the two imaged spectral bands was γ_{m1}=1 and γ_{m2}=0.43.

The autofluorescence of the bulk tissue was measured with no cylinder inside the slab. These measurements were subtracted from the measurements with the inclusion submerged in the phantom. An empirically measured noise level was used to reject too noisy data.

2.2 Fluorophore region confinement

It has previously been reported that the intensity ratio of two fluorescence spectral bands is dependent on the fluorescent inclusion position[7]. In the visible part of the spectrum this is due to the difference in bulk tissue attenuation, mainly influenced by the blood absorption[8]. This is experimentally shown in Fig. 2a-b) where the detected fluorescence emission at the boundary is shown for a fluorescent cylinder placed at two different depths inside the slab.

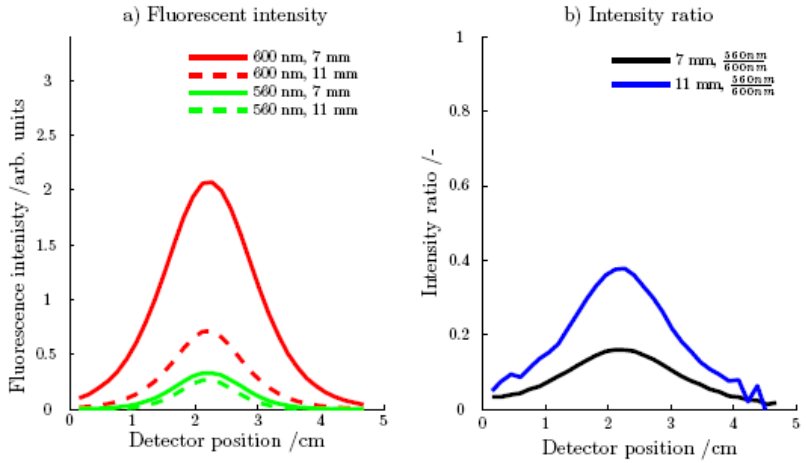

Figure 2. a) Fluorescent emission, at 560 nm and 600 nm, detected at the boundary from the same inclusion positioned at depth 7 and 11 mm respectively. b) Fluorescence intensity ratio, I(560)/I(600), of the two emission wavelengths detected at the boundary for two depths of the cylinder. The depth is defined in positive z-axis, see Fig 1.

The fluorescence emission intensity at a position $\mathbf{r}_d$, induced at a location $\mathbf{r}$, due to an excitation light source in $\mathbf{r}_s$ can be described by the diffusion approximation to the radiative transport equation[9], seen in Eq. (1).

$$u_m(r_s, r_d, k_m) = \frac{P_0}{4\pi D_x} G_x \eta_m(r) \frac{v}{4\pi D_m} G_m \tag{1}$$

where G_x and G_m denotes the Green's function to the homogeneous diffusion equation for excitation light (x) and fluorescent emission (m) respectively, i.e.

$$G_x = \frac{1}{|r - r_s|} \exp(ik_x |r - r_s|) \tag{2}$$

and

$$G_m = \frac{1}{|r_d - r|} \exp(ik_m |r_d - r|). \tag{3}$$

P_0 is the excitation laser power, v is the speed of light in the medium, η_m is the product of the fluorescent quantum yield (γ_m) and the fluorophore absorption coefficient (μ_{af}). $D_{x,m}$ denotes the diffusion coefficient, adopted from Ripoll *et. al.* [10], which extends the diffusion approximation to high absorbing media. The diffusion coefficient is

$$D_{x,m} = v/\left(3\left(\mu_s'^{x,m} + \alpha\mu_a^{x,m}\right)\right). \tag{4}$$

The constant α is approximately 0.5 for the present set of optical properties[10]. The diffusion wave number ($k_{x,m}$) is given by

$$k_{x,m} = \sqrt{-\frac{v\mu_a^{x,m}}{D_{x,m}}}. \tag{5}$$

The probability for inducing a fluorescent photon at wavelength λ_{m1} or λ_{m2}, in a location $\mathbf{r}$, is given by the fluorescent quantum yield γ_{m1} or γ_{m2} respectively. As previously mentioned the intensity ratio of the two

spectral bands is dependent on the propagation distance. The intensity ratio is mathematically stated in Eq. (6).

$$u_{mR}(r,r_d)=\frac{u_{m1}(r_s,r_d,k_{m1})}{u_{m2}(r_s,r_d,k_{m2})}=\frac{D_{m2}\gamma_{m1}G_{m1}}{D_{m1}\gamma_{m2}G_{m2}} \tag{6}$$

Hence Eq. (6) is the forward model, based on the diffusion equation, of the fluorescent intensity ratio induced in a location **r** and detected in detector position $\mathbf{r}_d$. Since the fluorescent light is originating from several locations within the geometry the detected light is given by the volume integral in Eq. (7).

$$U_{mR}(r_d)=\frac{U_{m1}(r_d)}{U_{m2}(r_d)}=\int_V d^3 r u_{mR}(r,r_d) \tag{7}$$

By discretizing the geometry the integral is approximated by a summation and the fluorescent light is effectively the sum of all the voxels within the fluorophore region[9].

In order to calculate Eq. (6) in all voxels of the geometry the reciprocity theorem is considered[11]. This states that the fluence rate at $\mathbf{r}_d$ due to a point source in **r** is effectively the same as the fluence rate in **r** due to a point source in $\mathbf{r}_d$. For Eq. (6) this means $u_{mR}(r,r_d)= u_{mR}(r_d,r)$. The calculation of Eq. (6) is depicted for four detectors in Fig. 3 a-d).

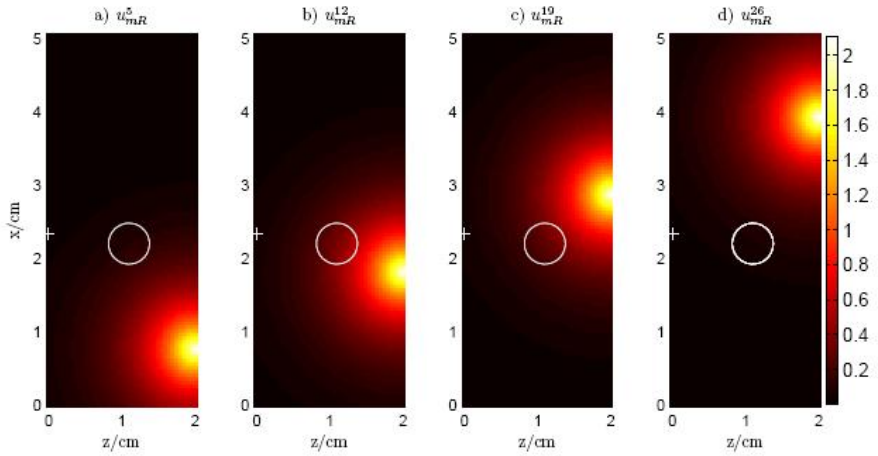

Figure 3. u_{mR}, defined in Eq. (6), for detector a) 5, b) 12, c) 19 and d) 26. The circle marks the true position of the fluorophore, inserted here for reference. The source position (+) and detector position (·) are also shown.

Figure 3 a-d) describes modeled intensity ratio inside the geometry. Only the voxels that are within the fluorophore region, i.e. the circle in Fig. 3 a-d), are contributing to the fluorescent emission. Hence the difference between the forward modeled ratio, given by Eq. (6) and the detected intensity ratio, Eq. (7) should yield a minimum for these voxels. The difference to be minimized is shown in Eq. (8) for detector *d* and voxel *i*.

$$\Delta U^d_{mR}(r_i)=\left|\ln\left(u_{mR}(r_d,r_i)\right)-\ln\left(U_{mR}(r_d)\right)\right| \tag{8}$$

The calculation of Eq. (8) is shown in Fig. 4 for four detectors. It is seen in Fig. 4 that the minima of Eq. (8) occurs at a certain distance from the specific detector. Since the intensity ratio (Eq. (7)) is dependent on the propagation distance all voxels positioned at the same distance from the detector will yield a minimum value of Eq. (8).

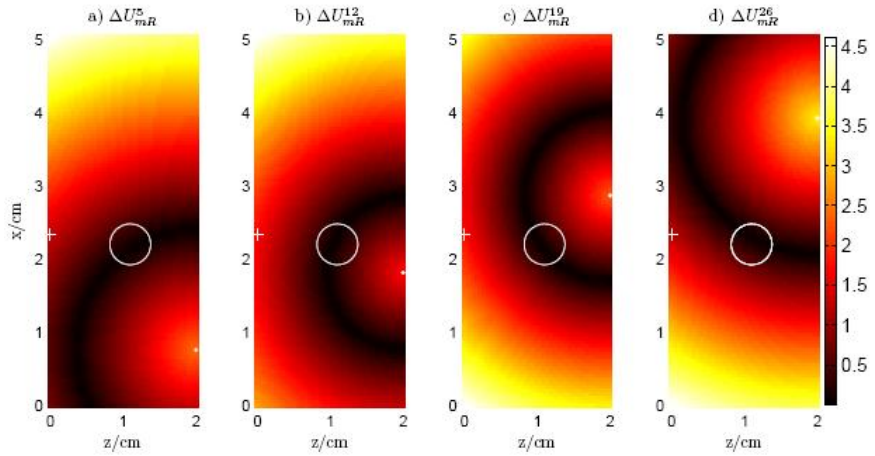

Figure 4. ΔU_{mR}, defined in Eq. (8), for detector a) 5, b) 12, c) 19, and d) 26. The circle marks the true position of the fluorophore, inserted here for reference. The source position (+) and detector position (·) are also shown.

By performing the calculations of Eq. (8) for all source-detector pairs and calculate the sum $\sum_{s=1}^{10}\sum_{d=1}^{31}\Delta U_{mR}^{d}(r_i)$ the fluorophore position is retrieved approximately where all the arcs, seen in Fig. 4, overlap. The summation is shown in Fig. 5a). In order to present a weight matrix of the geometry the summation was inverted and scaled so that the most probable fluorophore voxels were assigned 1 and the least probable voxels were assigned 0. The weight matrix is seen in Fig 5b).

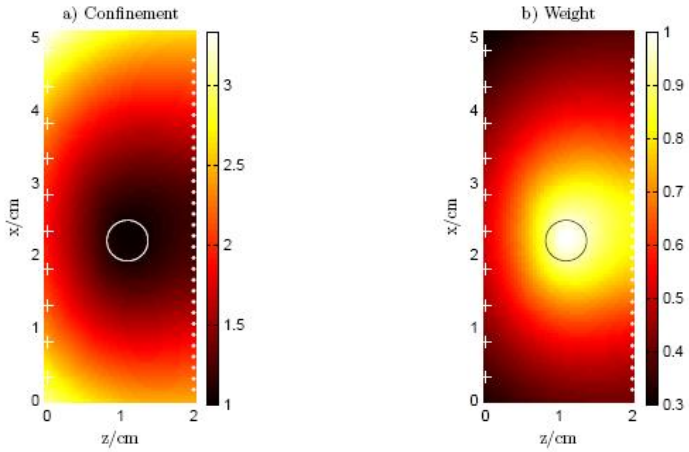

Figure 5 a) Summation of the arcs, b) Inverted and scaled weight matrix. Images are for a cylinder with inner diameter of 5.6 mm and 1 μM Rhodamine solution. All sources (+) are included as well ass all detectors (·).

2.3 Fluorophore position reconstruction using *a priori* information

In order to assess the performance of the method in a full reconstruction the normalized Born approach[12] was implemented. Here a set of linear equations, based on Eq. (1) can be formed using several source positions and several detector positions. The set of linear equations is then inverted to find $\eta_m(r)$, see Eq. (1), in every voxel building up the geometry. The set of linear equations is written as a matrix equation, i.e. $\mathbf{U}_{nB}=\mathbf{WX}$, where U_{nB} is the ratio between the detected emission light and the transmitted excitation light. X

is the vector comprised of all unknown $\eta_m(r)$ and W is a weight matrix where each element is given by the forward model, i.e.

$$W_{k,i} = \frac{u_m(r_{sk}, r_{dk}, k_m)}{P_0\left(4\pi D_x \mid r_{dk} - r_{sk} \mid^{-1} \exp\left(ik_x \mid r_{dk} - r_{sk} \mid\right)\right)} \tag{9}$$

where *k* is the source-detector pair and *i* is the voxel number.

To incorporate the prior information into the reconstruction each element in the weight matrix W was multiplied with the corresponding voxel-weight retrieved from the confinement, i.e. Fig 5b). Hence the voxels close to the fluorophore region has high weights while those voxels far from the fluorophore have smaller weights.

The set of linear equations was inverted using the algebraic reconstruction technique (ART) using 1000 iterations[12]. In each iteration run the absolute value of the error between the reconstructed and recorded fluorescence was assessed.

3. RESULTS

3.1 Single fluorescent inclusion

Fig 5a) shows the confinement of a single cylinder with inner diameter of 5.6 mm placed at a depth of 11 mm from the incidence plane. The concentration of the Rhodamine-phantom solution was 1 μM.

Fig. 6a-b) shows the confinement of the same cylinder, as above, filled with 0.5 μM Rhodamine-phantom solution placed at a depth of 7 mm from the incidence plane.

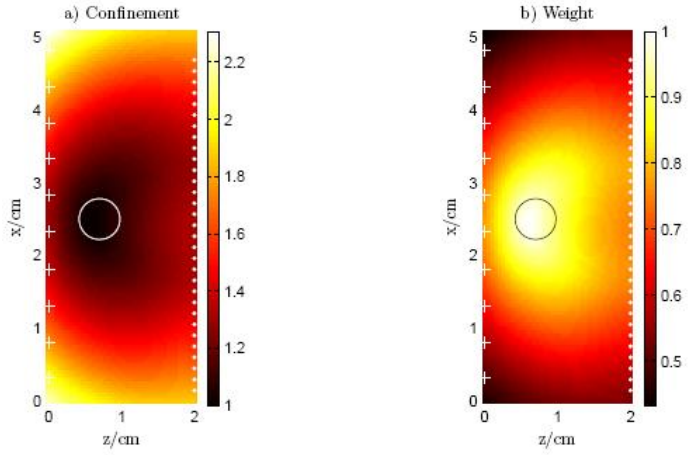

Figure 6 a) Confinement of a cylinder filled with 0.5 μM Rhodamine 6G-solution, inner diameter is 5.6mm, with center position 7 mm from the incidence plane. b) Weight matrix for the confinement in a)

3.2 Multiple fluorescent inclusions

Two identical cylinders, with an inner diameter of 5.6 mm, were placed at a depth of 9 mm from the incidence plane. The cylinders were filled with 1 μM and 0.5 μM of the Rhodamine-solution. The confinement and weight matrix is shown in Fig 7 a) and b) respectively.

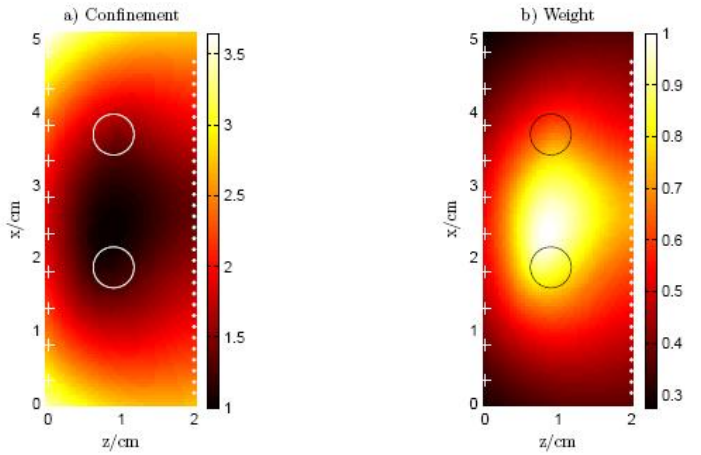

Figure 7 a) Confinement of two cylinders of inner diameter 5.6 mm. The lower cylinder is filled with 1 μM and the upper cylinder is filled with 0.5 μM Rhodamine-solution.

3.3 Reconstructions using prior information

The reconstruction of the two cylinders, presented in Fig 7 a-b) is shown in Fig 8 a-b).

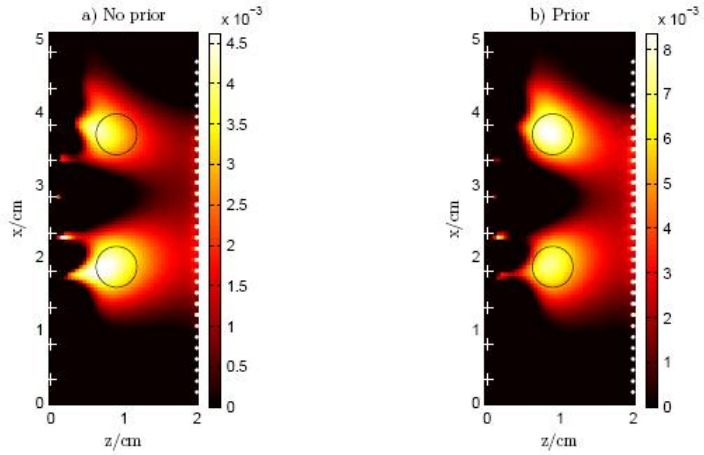

Figure 8. Reconstruction of two equally sized cylinders with different concentration using a) no prior information and b) prior information.

The reconstruction error, for each iteration, for the two reconstructions seen in Fig 8 a-b) is shown in Fig. 9.

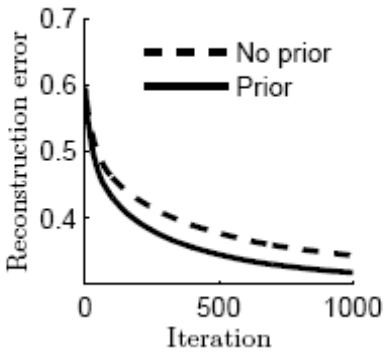

Figure 9 Reconstruction error for double cylinders, seen in Fig 8, with and without prior information.

4. DISCUSSION

The single cylinder confinements, seen in Fig 5 and 6, show a minimum for the true fluorophore position. It is seen that an inclusion positioned far from the detector boundary renders a larger confinement. This is mainly due to the decreased number of valid measurements due to longer propagation distance, i.e. more attenuated signals. Hence this effect is more prominent for detectors lying far from the fluorophore.

Fig 7a) shows a large confinement covering the region between the two cylinders. The lower cylinder, with the higher concentration, is closer to the minimum than the upper cylinder. The difference in signal strength is the most probable reason for this. The high concentration cylinder position is more accurately confined while the low concentration cylinder position is highly influenced by the fluorescence from the neighboring cylinder.

Despite the unsatisfactory confinement, in Fig. 7a), the weight matrix, in Fig. 7b), was used to impose weights on the voxels prior the inversion of the linear set of equations. The reconstructed result shows lower reconstruction error when using the prior weights. These initial results imply that it is feasible to use the prior weights, shown in Fig 7b). The reconstructions in Fig. 8 a-b) show artifacts around the inclusions but the center position is more accurately assessed with prior information. Looking at Fig 9 this is verified by the faster decrease of the reconstruction error.

The reconstructions presented herein only investigate the use of prior information to estimate the fluorophore position. The influence, of the method, on concentration reconstruction will be investigated in future studies. In the experimental setup used we subtracted autofluorescence from the measurements, something clearly not possible in *in vivo* imaging. It is of great importance the further investigate the influence of autofluorescence and also heterogeneous media. These studies are to be conducted in a near future.

5. ACKNOWLEDGEMENTS

This work was supported by the EU Integrated Project Molecular Imaging LSHG-CT-2003-503259.

REFERENCES

1. V. Ntziachristos, "Fluorescence molecular imaging," *Annual Review of Biomedical Engineering* **8**, 1-33 (2006)
2. R. B. Schulz, J. Ripoll, and V. Ntziachristos, "Experimental Fluorescence Tomography of Tissues With Noncontact Measurements," *IEEE Trans. Med. Imaging* **23**(4), 492-500 (2004)
3. E. Graves, J. Ripoll, R. Weissleder, and V. Ntziachristos, "A submillimeter resolution fluorescence molecular imaging system for small animal imaging," *Med. Phys.* **30**(5), 901-911 (2003)

4. E. Graves, J. P. Culver, J. Ripoll, R. Weissleder, and V. Ntziachristos, "Singular-value analysis and optimization of experimental parameters in fluorescence molecular tomograpy," *J. Opt. Soc. Am.* **21**(2), 231-241 (2004)
5. H. Xu, R. Springett, H. Dehghani, B. W. Pogue, K. D. Paulsen, and J. F. Dunn, "Magnetic-resonance-imaging-coupled broadband near-infrared tomography system for small animal brain studies," *Appl. Opt.* **44**(11), 2177-2188 (2005)
6. J. S. Dam, T. Dalgaard, P. E. Fabricius, and S. Andersson-Engels, "Multiple polynomial regression method for determination of biomedical optical properties from integrating sphere measurements," *Appl. Opt.* **39**(7), 1202-1209 (2000)
7. J. Swartling, J. Svensson, D. Bengtsson, K. Terike, and S. Andersson-Engels, "Fluorescence spectra provide information on the depth of fluorescent lesions in tissue," *Appl. Opt.* **44**(10), 1934-1941 (2005)
8. J. Svensson and S. Andersson-Engels, "Modeling of spectral changes for depth localization of fluorescent inclusion," *Opt. Express* **13**(11), 4263-4274 (2005)
9. M. A. O'Leary, D. A. Boas, X. D. Li, B. Chance, and A. G. Yodh, "Fluorescence lifetime imaging in turbid media," *Opt. Lett.* **21**(2), 158-160 (1996)
10. J. Ripoll, D. Yessayan, G. Zacharakis, and V. Ntziachristos, "Experimental determination of photon propgation in highly absorbing and scattering media," *J. Opt. Soc. Am. A* **22**(3), 546-551 (2005)
11. S. R. Arridge, "Optical tomography in medical imaging," *Inverse Problems* **15**, R41-R93 (1999)
12. V. Ntziachristos and R. Weissleder, "Experimental three-dimensional fluorescence reconstruction of diffuse media by use of a normalized Born approximation," *Opt. Lett.* **26**(12), 893-895 (2001)